BULLETIN OF THE POLISH ACADEMY OF SCIENCES
TECHNICAL SCIENCES, Vol. 70(3), 2022, Article number: e141000
DOI: 10.24425/bpasts.2022.141000

Research of damage to the rear wheel rim in a tipper-truck

Przemyslaw KUBIAK[1,2], Marek WOZNIAK[3], Sergiusz ZAKRZEWSKI[3], Krzysztof SICZEK[3]*, Adam RYLSKI[3], Adam MROWICKI[1], Jan MATEJ[1] Jakub DEDA[1] and Lech KNAP[1]

[1] Faculty of Automotive and Construction Machinery Engineering, Warsaw University of Technology, Narbutta 84, 02-524 Warsaw, Poland
[2] Ecotechnology Team, Lodz University of Technology, Piotrkowska 266, 90-924 Łódź, Poland
[3] Faculty of Mechanical Engineering, Lodz University of Technology, Stefanowskiego 1/15, 90-537 Łódź, Poland

Abstract. Serious damage to the inner rim of the rear twin wheel in one dump truck was noted during the operation of the fleet performing transport tasks. It was a drive wheel, and its damage occurred while driving with a load exceeding the permissible value. The examination of selected fragments of the damaged rim surface was conducted visually as well as using a digital microscope with a portable head. The measurements of the Vickers hardness and microscopic observations of the material structure of the sample cut along the thickness of the rim disk were carried out. The drive torque loading of the twin wheels of the tipper-truck rear axle, under their mating with different kinds of road roughness and under various vertical loads of the wheels was calculated. An analysis of stress distributions in the rim modelled using the Finite Element Method was also conducted for several possible scenarios of wheel loading. The damage to the rim was caused by simultaneous action of several factors, such as overloading the car, poor condition of the tires, loading the drive wheel by a part of the vehicle weight and the driving torque, and hitting a wheel on a cavity in a dirt road, causing a temporary relief of one of the tires on a twin wheel.

Key words: tipper-truck; rim; tire; failure.

1. INTRODUCTION

Nowadays, for the transport of some bulk materials, such as sand or gravel dump trucks are used. The chosen means of transport depends on the properties of the transported material (sensitivity to weather conditions, etc.). Work with bulk materials is most often undertaken by specialized companies that have the necessary machines at their disposal and transport cargo by road [1], but also in off-road conditions with varying degrees of terrain obstacles. According to [2], such companies' profits are affected mainly by the fuel consumption of individual vehicles, the driver (driving style), and the year season (average temperature, weather conditions).

The cargo is transported under the conditions of varying loads of the vehicle wheels on the side of the road or terrain, the weight of the cargo and the evenness of its distribution on the vehicle, and the driving style, often dictated by the changing road conditions.

Failure analysis seeks to identify and explain the causes of failures using scientific and technological concepts and principles. It is a transversal area of engineering with a great interest for the industry since the study of failures helps their prevention [3].

The failures of wheels of tipper trucks were related to their rims [4–20] and tires [21–34]. The latter are affected by the age of tires [35–38] and the tire-road friction coefficient [39–58].

*e-mail: ks670907@p.lodz.pl

Manuscript submitted 2021-07-09, revised 2022-01-13, initially accepted for publication 2022-03-03, published in June 2022.

The root cause of the problem was analyzed as follows: one of the transport companies, which deals with the transport of construction goods, encountered the necessity of fast, but short-term transport of cargo in the form of pallets with paving stones. The only means of transport available at that moment, capable of accommodating the required number of pallets with a paving slab, turned out to be a long-mileage tipper-truck (Fig. 1), the tires of which were heavily worn, and therefore the car was rarely used.

Fig. 1. The analyzed Mercedes-Benz Actros 4143 K 2002 tipper-truck with the damaged wheel replaced

As the destination distance was relatively short (about 10 km), the company decided to take the risk, being fully aware that the transport would take place under the conditions of exceeding the permissible loads of the tipper axle. The vehicle covered most of the distance on a sub-urban asphalt road, in light traffic conditions on a cloudy, but not rainy day. There were no noticeable signs indicating an impending failure. Only after leaving

the asphalt road and going onto a dirt road (Fig. 2), which was the driveway to the unloading site, there was a failure on one of the twin wheels of the rear axle of the vehicle (Fig. 3).

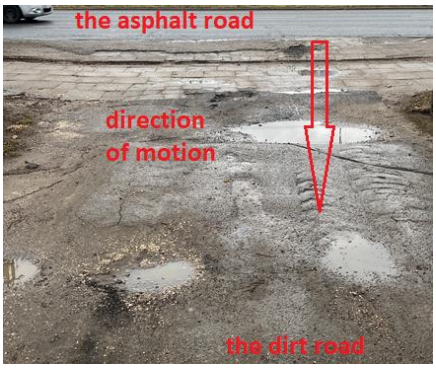

Fig. 2. The place of the analyzed traffic issue on the dirt road after leaving the asphalt road

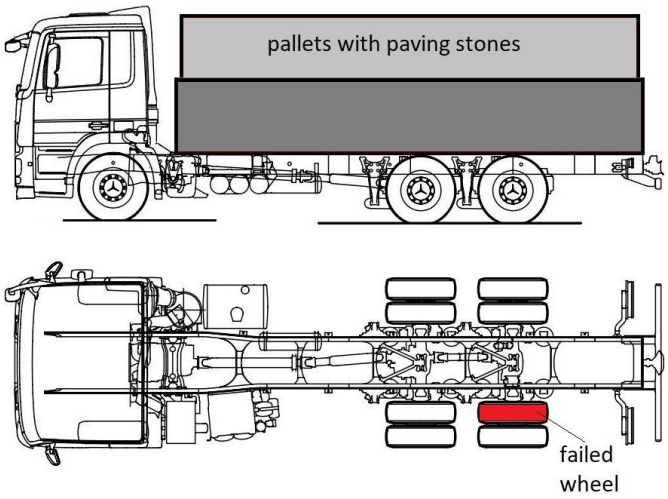

Fig. 3. The position of the failed outer tire of one of the twin wheels of the rear axle of the tipper-truck

The inner tire simply burst off. Moreover, the rim of this wheel was severely damaged (Fig. 4). Interestingly, the outer tire and rim of this twin wheel were not damaged. There was also no visible damage to the drive shaft, despite exceeding the permissible axle load. Described observations prompted the authors to look for the cause of such damage to the wheel, especially its rim.

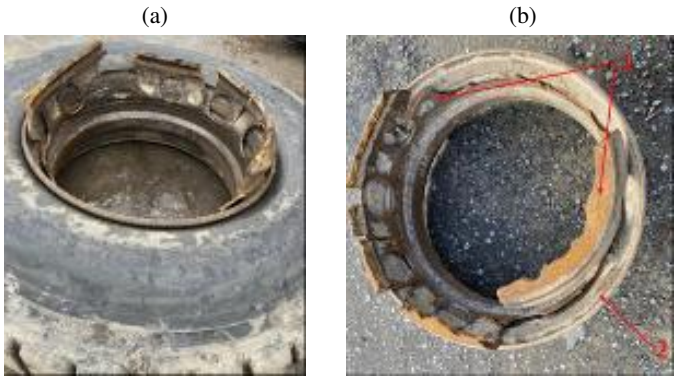

Fig. 4. The failed wheel with the damaged rim: (a) with a tire; (b) without a tire, 1 – fragment of the damaged rim, 2 – fragment of the rim that is free from damage

2. EASE OF USE

There are four main aspects of the failure of the rear wheels of the tipper truck: rim failure, tire failure, tire age, and tire-road friction coefficient. The other factors such as tire air pressure, condition of the rim mounting bolts, and wheel hubs were controlled on an ongoing basis and it was found that their effect on the failure can be considered negligible in further analysis. On the other hand, the wheels on the truck were frequently replaced during the operation of the vehicle, and therefore the condition of their tires and rims, as well as the friction conditions between the road and the tires, were subject to significant changes and could have had the greatest impact on damage to the wheel. The effect of the load on the wheel failure was partially included in the analysis of the stresses generated in the rim model, described further in the paper. The influence of the wheel's rotational speed on the damage was neglected because the accident took place on an access road, during intensive maneuvering of the vehicle on a relatively short stretch of dirt road.

2.1. The features and failures of the rims utilized in various vehicles

Panjagala *et al.* [4] stated that the wheel rim strongly affects the vehicle dynamics. They discussed the design and model of different wheel rims based on weight optimization. They found that Al alloys are the most suitable for the sport utility vehicles (SUV).

Carboni *et al.* [5] listed three typical problems of the track wheels components, in terms of fatigue strength:

- Disk failure caused by fretting fatigue in the attachment face zone.
- Crack nucleation and propagation at the edge of the ventilation holes where the maximum circumferential stress exists (at 45° to the axial direction).
- Fatigue failure of the welded joint between disk and rim.

Varin [6] reported that the number of vehicle accidents affected by wheel attachment failures on non-dual rear wheel vehicles increased after introducing the cast and forged aluminum alloy and forged "styled" steel wheels. An increase in such accidents in the case of solid wheels was related to a common failure since the stiffer cast and forged wheels required more stringent installation and maintenance standards than the stamped steel predecessors. Coincident with, but not in response to, the increased number of wheel attachment failures on single rear wheel vehicles was the introduction of hub-piloted wheels. Those were applied on dual rear wheel vehicles to limit the higher frequency of attachment failures on vehicles equipped with forged steel wheels. It enhanced the portion of the installation torque converted to wheel clamping force through a weakening in the portion lost to nut-to-wheel friction. The wheel-clamping force occurs, as the tightening with a specified torque value of the nut mating with the stud results in the generation of

the longitudinal stresses in the core of the wheel stud on a car. The integration over a stud cross-section of such stresses results in a force equal to a clamping force component related to the single stud. The sum of such components, the number of which is equal to that of the studs is the clamping force that holds the wheel to the hub.

Glennon [7] reported that crashes caused by wheels coming off of vehicles referred to as wheel runoff crashes can be caused by a failure of:

- The wheel mounting system, such as the wheel studs, lug nuts, etc.
- The hub and wheel bearing assembly.

Prasad *et al.* [8] stated that wheel rims can be made of Al alloys, Mg alloys, Steel 1008, forged steel, and Carbon fibers.

Natrayan *et al.* [9] conducted numerical studies on old and new wheel rims made of various materials. They found that deflections in aluminum rims were greater compared to ones made of stainless steel. They suggested that stainless steel is preferred as the best material for wheel rim.

Sabari et. al [10] numerically compared deformations of the wheel rims made from carbon steel and aluminum alloy, under various loads and cruising speeds. It was found that with the increase in speed, the maximum deformations of both materials also increased. Deformations of wheel rims made of aluminum alloy were greater compared to those for rims made of steel.

In [11] various types of wheel rim materials, particularly aluminum alloys, were compared. It was found that basic requirements for the rim material are strength, structural stiffness, fatigue behavior, and crashworthiness. Zhang *et al.* [12] studied a range of casting-related defects in low-pressure die-cast aluminum wheels, which affected three main casting quality-related criteria for automotive wheels: cosmetics, airtightness, and mechanical performance.

Stanczyk and Filgus [13] reported that the 6082 aluminum alloy was intended for use in loaded machine parts and forged car wheel rims.

Satyanarayana and Sambaiah [14] numerically studied the fatigue behavior of the wheel rim made of overcast aluminum alloy (Al.356.2) under constant loading.

Sourav Das [15] investigated the wheel rim made of the AlSi7Mg0.3 alloy and Ganesh and Periyasamy [16] studied the spiral wheel rim made of the Al356.2 alloy. Such authors found that the bent magnesium rims cannot be repaired.

Wang *et al.* [17] proposed a method for evaluating the fatigue life of aluminum wheels. They found that during the aluminum wheel rotary fatigue bench test, the baseline wheel failed the test, and its crack initiation was around the hub bolt hole area. Toulfatzis *et al.* [18] conducted a failure analysis of an Al-alloy wheel rim, showing a transverse and axial fracture. They found a localized dent due to the occurrence of intense plastic deformation adjacent to the fracture area. No significant macro-defects occurred that could cause the overload fracture of the wheel rim, rather than an impact incident able to induce a high strain-rate loading crack propagation that resulted in the ultimate failure.

Surasno and Tjahjohartoto [19] conducted comparative tests of various rims made of casting aluminum alloy made by the small and medium-sized enterprises (SMEs). Their tensile strength was much lower than these of local and imported products. Their impact values resulting in rim break were lower than the Indonesian National Standards (2008) SNI 1896, Tire Rims for Category M, N, and O Motor Vehicles (SNI 1896:2008) requirement. Their content of iron was higher than these of local and imported rim, tending to form micro-cracks and limit the mechanical strength. Microstructure observation revealed a dendritic structure, porosity, and a needle-like AlFeSi phase.

Kwak *et al.* [20] numerically analyzed the process of the Al alloy wheel impact test for both the wheel models with and without shrinkage cavity defects. They found that under impact test conditions, the wheel with modeled shrinkage cavity defects may fracture while the sound-assumed wheel may not.

It is visible that studies on rims made from Al alloys are performed much more often than those made of steel. Although the deflections in steel rims are lower compared to aluminum ones, both can be damaged due to the possible fatigue phenomena. Also, the bad technical conditions of the wheel mounting system, such as the wheel studs and lug nuts can cause wheel failure.

2.2. The failures of the tires utilized in various vehicles

Liu *et al.* [21] studied the effects of heat accumulation and stress distribution on the run-flat tire sidewall on durability testing at zero pressure. They found that the rigidity and tensile strength of the compound were negatively correlated with temperature. The deformation strongly affected energy loss and the stress concentration could cause early damage to the tire. The balance of mechanical strength, energy loss, and structural rigidity allowed the optimal development of run-flat tires.

According to [22], very common types of tire damage are punctures, cuts, cracks, bulges, or irregular wear.

Edunyah [23] reported that there were four major causes of tire failure: over-inflation, under-inflation, wear, and overloading of the vehicle.

The improper maintenance of vehicle tires adversely affected vehicle acceleration, braking, steering, comfort, and efficiency, and in some cases lead to crashes [24]. The tire rubber and other compounds become brittle, resulting in loss of grip, and enhancing the risk of catastrophic failure.

In [25], the authors discussed a specific vehicle and wheel model. Simulation results of rupture propagation and tire interaction were obtained. Based on those results, two interesting modifications were proposed to increase the strength and resistance of the tire structure. This modification could potentially be applied to utility trucks.

Another wheel design was proposed in [26]. The authors proposed the structure of an ultra-high-strength tire and studied the effect of using such a tire on vehicle vibrations and ride comfort. The study showed that this type of tire reduces comfort, but a significantly improved grasping ability was achieved.

Weyssenhoff *et al.* [27] reported that some tires have hidden defects arising from production process errors. Such defects resulted from nonuniformity of the tire structure and translated into improper operation and could even lead to an accident.

The material nonuniformity can adversely influence tire-road interaction: the enhanced noise level generated, as well as sus-

pension vibrations or transmitting vibrations to the steering column [27–29]. Dorfi [30] found that such vibrations are sensed by the driver only in a certain range of the vehicle speed. Such vibrations may initiate resonance of the vehicle steering system, as the wheel is unbalanced. In extreme cases, tire defects can lead to a burst of its structure. Such an anomaly weakens the safety level and comfort [27].

Weyssenhoff *et al*. [27] also pointed out that the inadequate wheel balance causes improper wear of the tire tread surface. In addition, radial run-out due to tire nonuniformity may introduce resonant frequency causing perceptible vibrations on the steering wheel for the specific speed ranges.

Drivers, despite being aware of the risks of improper inflation, often run vehicles with underinflated tires [31], and for less well-known issues such as tire aging, oxidation, and cracking, drivers are unaware of the need for replacement [24], forgoing the inspection entirely.

Euchler *et al*. [32] studied the crack initiation during a dynamic wear process and its correlation with fatigue crack growth of reinforced rubber materials. They analyzed rubber compounds based on natural rubber (NR) and polybutadiene rubber (BR). They found that the crack initiation process during dynamic wear depended on different impact energies and the rubber compositions. The higher crack initiation resistance of rubber blends occurred with an enhanced content of BR, while a predominant effect of NR increased the resistance against crack propagation, especially at higher strain levels due to strain-induced crystallization.

Zhang *et al.* [33] proposed a method of tire damage image recognition based on a convolutional neural network algorithm and elaborated on an intelligent tire damage image recognition system. Siegel *et al.* [34] proposed a monitoring system of tire surface conditions using a densely connected convolutional neural network to identify cracking based on smartphone images.

It is visible that failures of tires may be caused by external factors, for example, punctures, cuts, and internal ones such as tire aging, oxidation, and cracking. The latter depends on impact energy and the rubber composition. The tire failure can be accelerated by improper inflation, wear, and overloading of the vehicle. The improper maintenance of tires causes the brittleness of their rubber and other compounds and the generation of hidden defects during the production process can induce the enhanced level of noise generated and suspension vibrations transmitting to the steering column. The mentioned defects can lead to a burst of the tire structure and the inadequate wheel balance leads to improper wear of its tread surface. It has been also noticed an increased role of tire state monitoring systems.

2.3. The age of a tire

By conducting an artificial aging process of the tire and periodical testing, Wright and Els [35] studied the effects of a tire age on its stiffness parameters. Researchers have applied simplified methods of quantifying the age of the tire to update a flexible structure tire model (FTire model). It was a full 3D nonlinear in-plane and out-of-plane tire simulation model [36]. Wright and Els found that the vertical and longitudinal stiffnesses of the tire depend on its age. The application of the Shore A hardness of the tire tread to update the FTire model was useful to account for the age of the tire. The changes in tire properties due to aging were small but not negligible. The error between a severely aged tire and a tire model based on a new tire was below 5%.

In [37] some facts were reported related to the aging effect on the tire conditions:

- Rubber, which is also utilized in tires, started breaking down over time and heat accelerated this process, which was referred to as tire aging.
- Despite the small wear of the tire, that is, the tread of the tire was of significant depth, and the violation of its integrity started. The effect of aging might be visibly undetectable.
- Tires aged whether they were driven on or not. Therefore, the problem occurs also when the vehicle was used infrequently or in the case of spare tires.
- With the development of their age process, tires were more prone to failure.
- Some tire manufacturers recommended replacing tires with their age in the range of 6-10 years, regardless of tread wear.

Balderstone *et al.* [38] identified an increase in stiffness of tire rubber compounds that occurs due to the aging process. This was also associated with a decrease in elasticity. Some tires returned from service exhibited anomalies associated with the steel belts, whereas no anomalies occurred in the new or new/thermally aged tires. The looseness of the belts in the mentioned package, being a breakdown of the steel-cord and rubber compound, could cause rejection of components in the unpredictable moment in the retreading process.

The authors also reported a peel force reduction that occurred in the first three to four years of tire life. Peel force visibly decreased within that age range, for belts 2 to 3, belts 3 to 4, and between the carcass and sidewalls, as compared to a new tire. However, following the initial decrease of peel force, there was no further significant reduction over the age range of the service tires. The thermally aged tires also exhibited the reduced peel force compared to the control tire; however, not so much as the service tires.

Some tires returned from the service exhibited corrosion of the steel cords, especially in the outer belt of the tire structure. That corrosion was probably due to penetrations throughout the tread of the tire. Apparently, they were not deep enough to penetrate the inner layers or puncture the tire. Such corrosion weakened the bond between the steel cords and its coating made of adhesive rubber compound and affected the integrity of the tire in service, which may cause its malfunction.

Based on the observations stated in the articles on the tire aging, it can be concluded that in the analyzed case there could be enough damage to the cord when driving with a load on unpaved roads or various types of ramps to construction sites or farms. Abandoned various sharp objects, such as nails, rod fragments, wires, sharp chippings, or stones, which are often found there, could be potential sources of tire punctures. Intensive use of vehicles and inaccurate compliance with periodic tire changes, due to the additional costs and losses related to the need to send the vehicle to the workshop, could have resulted in significant wear of the treads.

2.4. Maintaining the integrity of the specifications

When driving a vehicle, the occurrence of the conditions conducive to rolling its wheels on the road, without the occurrence of longitudinal and lateral slips, is desirable. However, a long-term practice shows that while driving, there may exist various slips differing from each other in the direction and values of their speed components [39]:

- Longitudinal slip of wheels during, for example, vehicle braking
- Slipping of driving wheels when starting or accelerating the vehicle
- Lateral slipping of vehicles during, for example, a vehicle turning, side gusts of wind, unsymmetrical wear of the wheel treads

According to [40], a vehicle experiences only tire-road forces strongly affecting its lateral, longitudinal, yaw, and roll behavior. For each tire, the normalized traction force ρ, called the coefficient of traction, is defined via equation (1) [40]

$$\rho = \frac{\sqrt{F_x^2 + F_y^2}}{F_z}, \tag{1}$$

where: F_x, F_y, and F_z are the longitudinal, lateral, and normal, that is, vertical, forces acting on the tire. For a given normal vertical load on the tire, the maximum value of the normalized traction force ρ, called the tire-road friction coefficient μ, depends on the characteristics of the road surface. The value of μ varies in the range $\langle 0, 1 \rangle$ depending on the type of road surface, such as icy, snow-covered, gravel, and dry asphalt.

Some methods were developed to estimate the tire/road friction coefficient. Ghandour *et al.* [41] proposed a method for the estimation of the maximum tire/road friction coefficient, based on an iterative quadratic minimization of the error between the developed lateral force and the model of tire/road interaction. Fodor *et al.* [42] devised a numerical model for the evaluation of different tire-road friction estimation methods such as:

- The Slip-Slope Method utilizing the relationship between normalized longitudinal tire force and slip ratio to determine the friction coefficient
- The Cornering Stiffness Method detecting the maximum the friction coefficient
- The Burckhardt Method based on a special formula

Chen and Wang [43, 44] proposed a real-time, tire-road friction coefficient estimation method that is independent of vehicle longitudinal motion for ground vehicles with separable control of the front and rear wheels.

Ahn *et al.* [45] reported two methods to estimate the friction coefficient: the first based on lateral dynamics, and the second based on longitudinal dynamics.

For the algorithms estimating independent friction coefficients for each wheel of the vehicle, Rajamani *et al.* [46] devised three different observers for the estimation of slip ratios and longitudinal tire forces, based on the types of sensors available.

Cheng *et al*. [47] proposed an observer using the unscented Kalman filter to estimate simultaneously the sideslip angle, lateral tire-road forces, and the tire-road friction coefficient.

For estimating the peak friction coefficient in the tire-road interface, de Castro *et al*. [48] proposed a parametrization based on a feedforward neural network (FFNN), trained by the extreme learning machine (ELM) method.

Some studies addressed the effect of different parameters on the friction coefficient in the tire-road contact zone.

Liu [49] studied the adhesion coefficient of an automobile tire and road surface. A formula was proposed for the adhesion coefficient comprising of two parts: adhesion and deflective. The formula takes into consideration several factors: road surface state, tread rubber properties, tire geometry, tire air pressure, wheel normal loading, and road surface roughness. It was found that the adhesion coefficient is a function with an extreme value. Under conditions of the atmospheric pressure in the tire, improper selection of the load of the vehicle, and the roughness of the road surface, such a function can reach its lowest values and affect the safety of the driven vehicle.

The adhesion coefficient in the contact zone between the tire and road depends on the kind of road and its wetness [50]. It is also influenced by the vehicle speed and the tread depth [51].

Cabrera *et al*. [52] reported that the road friction resistance depends on road composition and wet conditions, tire type, and its features. They proposed a modification of the Pacejka Magic Formula to include the effects of road composition and its state, tire type, vehicle speed, and slip between the tire and the road. It facilitated obtaining a more accurate tire-road friction model.

Acosta *et al.* [53] reviewed road friction virtual sensing approaches. The road grip potential can be estimated accurately under regular driving conditions in which the vehicle responses remain within low longitudinal and lateral excitation levels. To reach this goal, the effect-based estimation methods based on tire slip, tire vibration, and tire noise are used, in which the road friction characteristics are obtained from the tire responses.

Lian *et al.* [54] reported that the tire-road friction coefficient is not measured directly. Some methods are devised to experimentally determine the values of friction coefficient in tire-road contact. The authors also discussed the tire force system and the developing status of the identification of tire-road friction conditions involving the approach based on sensor equipment and the approach utilizing the measurement of the vehicle motion, and some classical identification algorithms used in this field.

Erdogan *et al.* [55] proposed a tire-road friction coefficient estimation using the uncoupled lateral deflection profile of the tire carcass measured from inside the tire through the entire contact patch. The decoupling of the lateral carcass deformations from the radial and tangential deformations was possible using the wireless piezoelectric sensor.

Erdogan *et al*. [56] devised an adaptive feedforward vibration and cancellation-based system of friction estimation facilitating a continuous measurement of the friction coefficient under all vehicle maneuvers, even without its longitudinal and lateral accelerations. The real-time knowledge of friction coefficient in tire-road contact is important for issues related to the operation of various active safety control systems including adaptive cruise control (ACC), anti-lock braking systems (ABS), electronic stability program (ESP), and acceleration slip regulation (ASR). However, the tire-road friction coefficient is not measured directly [54].

According to [57], the tire-road friction conditions affect the vehicle control systems, particularly, the wheel slip control systems. The knowledge of the actual maximum coefficient of friction allows an anti-lock brake system (ABS) controller to start braking with the optimal brake pressure, resulting in shorter stopping distances.

Lex [58] reported that the driver input conditions the vehicle reaction, depending on the road and tire conditions. That also held true for the advanced driver assistance systems (ADAS), whose operation was usually based on the wheel rotational speeds, as they exhibited the highest sensitivity to the road and tire conditions.

The conducted literature review on the coefficient of friction between the tire and the road showed that the tire-road friction coefficient μ depends on the characteristics of the road surface. The value of μ varies in the range $\langle 0, 1 \rangle$ depending on the type of road surface, such as icy, snow-covered, gravel, and dry asphalt. For estimation of the mentioned coefficient, there are some methods based on measuring systems or numerical simulations with various levels of accuracy and repeatability. The lack of a wheel slip control system or the insufficient efficiency of such a system deteriorates the driving conditions of a vehicle, especially a multi-axle vehicle, such as that analyzed in the present study.

3. MATERIALS AND METHODS

3.1. The general view of the damaged wheel

The examination of the failed wheel was carried out visually at the accident site. Also, the interview with the participants of the road accident relative to the cargo transportation conditions was made. Additionally, the examination of selected fragments of the damaged rim surface was conducted visually and by using a digital microscope VHX7000 manufactured by the VHX Keyence.

3.2. Testing of the mechanical properties of the damaged rim material

The wheel rim analysis was made by welding the hub rim with its disc. Such a connection was conditioned by making the components of the hub from weldable steel with a carbon content below 0.3 wt.%.

Hardness tests and microstructure tests of the rim material were carried out. For this purpose, a piece of material was taken along the thickness of the rim disc from the area between the hole for the wheel hub and the hole for one of the rim mounting bolts. The above-mentioned material sample and positions of the measurement points are shown in Fig. 5.

The hardness tests were carried out using the Vickers method with a load of 98.1 N, on an INNOVATEST hardness tester, model VERZUS 700. In each case, 5 hardness measurements were made and the presented values were calculated as average ones.

The obtained values of the hardness HV facilitated the estimation of the fatigue strength σ_w for the steel according to equation (2) [59]

$$\sigma_w \cong 1.6 \cdot HV \pm 0.1 \cdot HV \quad \text{for} \quad HV \leq 400. \tag{2}$$

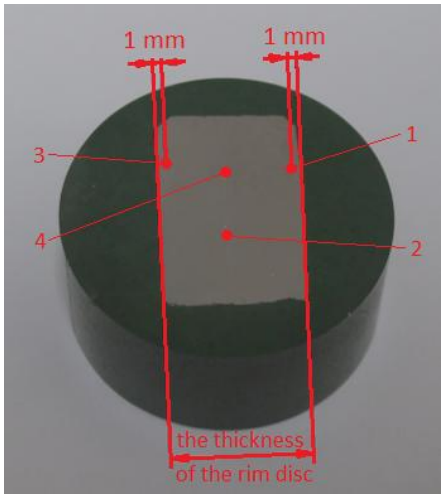

Fig. 5. The material sample cut along the thickness of the rim disk to measure the surface hardness at selected disk depths and to examine the metallographic structure of the sample; 1 and 2 – points for measurement of the hardness, 3 and 4 – points for tests of the microstructure

Microstructure tests of the rim material were carried out on the sample taken both at the outer surface of the rim and in the center of the cross-section using the MA 200 optical microscope by NIKON.

3.3. Characteristics of the vehicle analyzed

The presented study was conducted for the Mercedes-Benz Actros 4143 K 2002 tipper-truck (Fig. 1) with a capacity 20 m^3 related to a loading capacity of 22 800 kg [60]. Its total weight was 40 000 kg. It was equipped with the CI turbocharged V6 320 kW Euro 3 engine with displacement of 11 946 cm^3 and a 16 gears manual transmission. The characteristics of the engine, such as power $P(n)$ and torque $M(n)$ as a function of engine speed n were presented in Fig. 6. The maximum torque $M_{\max}$ was equal to 2100 Nm at the engine speed $n_{M_{\max}}$ equal to 1080 rpm and the maximum power $P_{\max}$ was equal to 320 kW at the engine speed $n_{P_{\max}}$ equal to 1900 rpm [61]. The 1st gear i_{gI} was equal to 11.72 and the 14th gear i_{gXIV} was equal to 1 [62]. The axle ratio i_a was equal to 5.333 [62]. The wheels possessed tires of the type 14.00 R20 with advanced rims [62] and therefore the radius r_d of the wheel was equal to 0.578 m [63]. The air pressure there was equal to 7.6 bar [63].

The torque $T_{P_{\max}}$ at the engine speed $n_{P_{\max}}$ was equal to 1620 Nm (Fig. 6).

The permissible rear axle mass $m_{\text{ra}-\text{perm}}$ was equal to 16 000 kg [62]. It was assumed the symmetrical transmission of drive torque through the twin wheels on the rear axle of the tipper-truck. The torque $T_{\text{ra}-\text{perm}}$ transferrable by the twin wheel of the tipper-truck rear axle loaded with a weight resulting from the permissible rear axle mass $m_{\text{ra}-\text{perm}}$ was determined from equation (3)

$$T_{\text{ra}-\text{perm}} = \mu \cdot \left(0.5 \cdot m_{\text{ra}-\text{perm}} \cdot g\right) \cdot r_d \,, \tag{3}$$

where: μ – the assumed tire-road friction coefficient during driving, equal to 1 on the dirt road and 0.6 on the asphalt road [50].

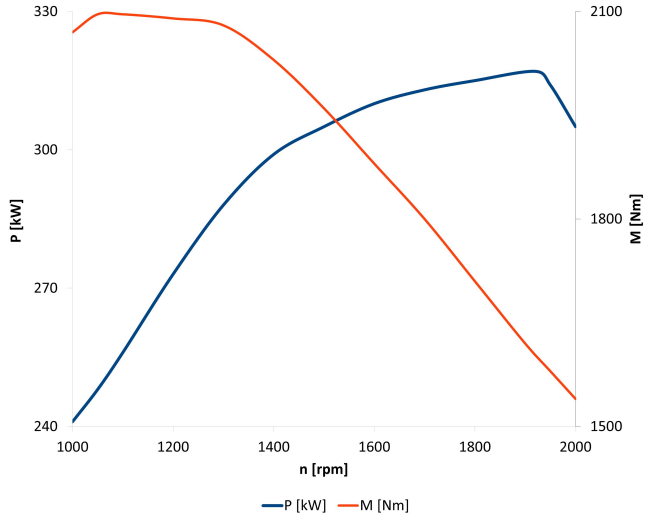

Fig. 6. The characteristics such as power $P(n)$ and torque $M(n)$ as a function of engine speed n of CI turbocharged V6 320 kW Euro 3 engine applied in the Mercedes-Benz Actros 4143 K 2002 tipper-truck

The maximal torque $T_{\mathrm{ra}-M_{\max}}$ acting on the twin wheel of the tipper-truck rear axle was determined from equation (4)

$$T_{\mathrm{ra}-M_{\max}} = T_{\max} \cdot i_{gI} \cdot i_a \,. \tag{4}$$

It was assumed that tipper drive on the asphalt road under conditions of the maximal engine power $P_{\max}$, with the use of the 14th gear i_{gXIV}. The torque $T_{\mathrm{ra}-P_{\max}}$ acting on the twin wheel of the tipper-truck rear axle was determined from equation (5)

$$T_{\mathrm{ra}-P_{\max}} = T_{P_{\max}} \cdot i_{gXIV} \cdot i_a \,. \tag{5}$$

During the transport of pallets with paving stones, the loading from cargo was equal to 48 000 t. This increased twice the loading of twin wheels of the tipper-truck rear axle. This led to reaching a value of $2 \cdot T_{\mathrm{ra}-\mathrm{perm}}$ by the torque transferrable by the twin wheel of the tipper-truck rear axle.

3.4. Model of the twin-rims assembly

The stress distribution in the assembly comprised of two rims of twin rear wheels of the rear axis and was obtained using the Finite Element Method implemented in the software Autodesk Inventor Professional v. 2021. The single rim was presented in Fig. 7. To carry out a numerical calculation of the model of the mentioned assembly was elaborated (Fig. 8). Each rim was made of weldable steel with a carbon content below 0.3 wt.%. It was assumed that the mechanical properties of steel AS/NZS 3679.1-300 [64] were very close to these of the steel applied to the rim analyzed. This assumption was supported by the fact, that during the initial (rough, due to the unsatisfactory technical condition of the used portable X-ray fluorescence (XRF) analyzer) analysis of the chemical composition of steel, an increased manganese content was observed. Also, from conversations with Mercedes-Benz truck dealers, information was obtained that the wheel rims are made of hot-rolled steel. The Yield stress for such steel was equal to 300 MPa, and the Tensile Strength was equal to 440 MPa [64]. The rims are connected by the plane interface covering the rim end faces (Fig. 8c). The corresponding pin holes / bolts in both hubs are coaxial with each other (Fig. 8b).

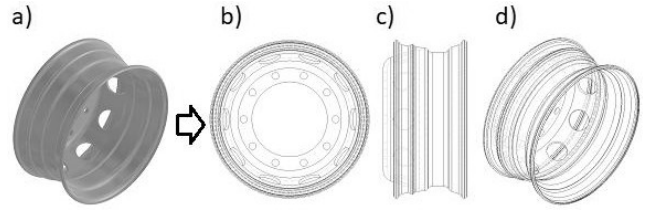

Fig. 7. The single rim utilized in the twin rear wheels of the rear axis of the tipper: a) general view; b) and c) wireframe style perpendicular views; d) wireframe style isometric view

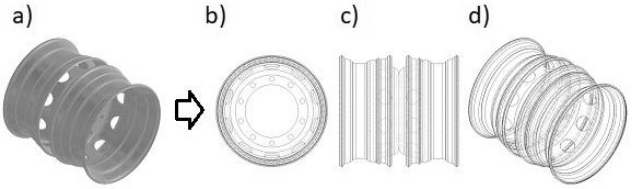

Fig. 8. The model comprised two rims of the twin rear wheels of the rear axis of the tipper: a) general view; b) and c) wireframe style perpendicular views; d) wireframe style isometric view

The contact elements were plane ones with the augmented option. The surfaces of the rims contacting with the wheel tires were fixed on one bottom half of their circumference (Fig. 9).

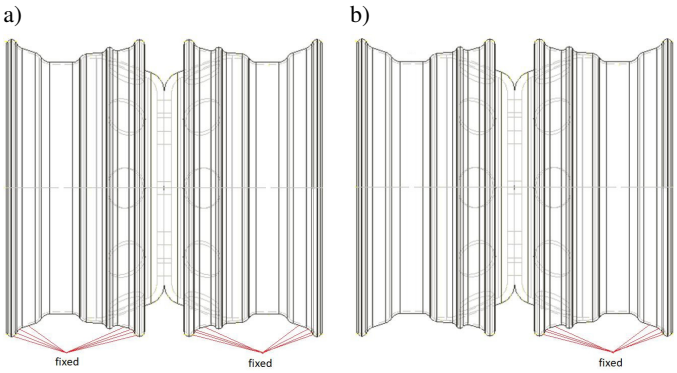

Fig. 9. The fixed surfaces of rims in the model of the twin rear wheels of the rear axis of the tipper: (a) the case when both twin wheels contacted the ground; (b) the case when only one tire of twin wheel contacted the ground

The common practice is that the rim is fixed in its holes and possibly on the inner surface of the hole [65–68]. The fixing of the rim surfaces, as in the present case, facilitates the introduction of changes in the rim load without the need to model a very complex and difficult element, which is the tire. However, it may introduce some rigidity of the analyzed rims concerning reality. Particularly large deviations would be achieved with rims made of aluminum alloys. Fortunately, in the analyzed case, the rims were made of steel, which is a much stiffer material. A similar method of confirmation as in the present analysis was used in [67, 69].

To simplify the analysis, the influence of compressed air pressure in the tire was also neglected. The presence and values of this pressure highly affect deformations of the tire [70, 71]. The presence of this pressure can increase the stress values in the rim by up to 50%, but to a very different degree depending on the pressure value and the circumferential direction of the rim [72]. The actual pressure in the twin wheel analyzed has not been known and it could even exceed its limit values. During the current analysis, the following principle was followed: if the calculated von Mises stresses in the rim caused by the load from the car weight and the driving torque exceed the plasticity limit of the rim material, they will exceed it even more if the influence of the presence of compressed air in the tire is considered.

Two cases were considered: the first one when both twin wheels contacted the ground (Fig. 9a) and the second one when only one tire of the twin wheel contacted the ground (Fig. 9b).

The maximal drive torque T was symmetrical, half its value, applied to the annular part of the plane of each hub containing the holes for pins/bolts connecting the twin wheels (Fig. 10). Half of the maximum vertical load G on the rear axle of the tipper by one twin wheel of this axle was applied to the same annular fragments of the plane (Fig. 10).

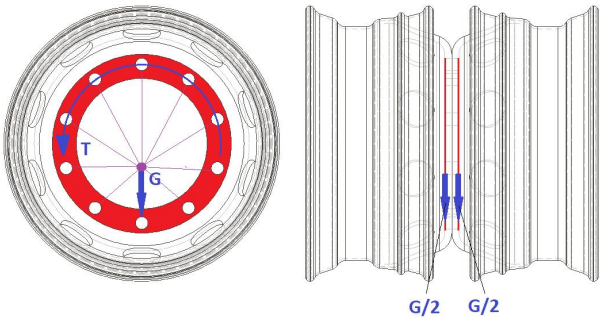

Fig. 10. The loading of rims in the model of the twin rear wheels of the rear axis of the tipper. T – the maximum drive torque, G – the maximum vertical load on the rear axle of the tipper by one twin wheel of this axle

The maximum vertical load G reached the value equal to a weight resulting from the permissible rear axle mass m $m_{\mathrm{ra-perm}}$, namely 16 0000 N.

The grid of the curvilinear 10-node tetrahedral finite elements was shown in Fig. 11. Five options of average element size were utilized to conduct convergence evaluation in terms of the effect of the average element size on the maximum values of calculated von Mises stresses. It was assumed that solution convergence can be obtained when the decrease of average element size results in the stabilizing of the maximum values of von Mises stress calculated for the same geometrical and material parameters, loads, and boundary conditions in the analyzed model. The parts included in the modelled assembly of rims had connected each other by contact elements with the option of 3D planar curvilinear 6-node triangles and the option of their bond behavior. It was assumed that during the analysis mating surfaces of rims did not move relative to each other. In real some micro-slides are possible, but they are quickly damped by the friction between such surfaces resulting from the interaction of their roughness under a strong pressure between them, caused by the tension of the bolts connecting the twin wheels. Therefore, such micro-slides were omitted for simplicity.

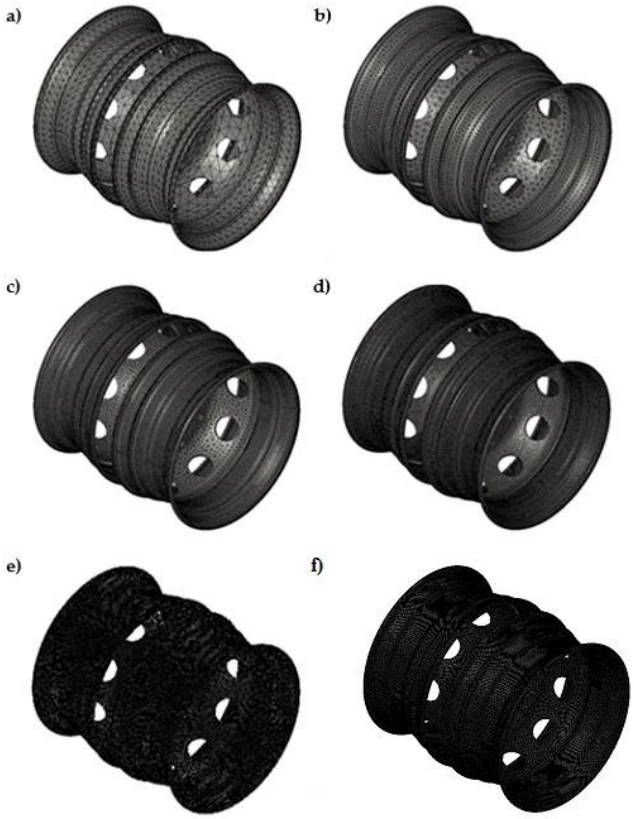

Fig. 11. The grid of tetrahedral finite elements. Average Element Size (as a fraction of bounding box length): a) 0.1 – 76857 elements, 153109 nodes; b) 0.05 – 93147 elements, 193671 nodes; c) 0.03 – 227881 elements, 470621 nodes; d) 0.02 – 457849 elements, 887356 nodes; e) 0.01 – 2917447 elements, 4841588 nodes, f) 0.005 – 7402836 elements, 11653415 nodes

3.5. The effect of the rim material parameters chosen and load on the achievement of its fatigue strength

The fatigue failure of any device usually occurs after several withstood cycles and is determined experimentally for the given geometrical and material parameters of the analyzed device and its operational conditions, particularly values of load and its manner of influence [73]. During the fatigue analysis of the rim, Sachin *et al.* [74] reported that a crack was initiated at $2.17 \cdot 10^5$ cycles for the rim made of steel alloy and at $1.97 \cdot 10^5$ for that made of the forged steel. Topaç *et al.* [75] reported that crack initiation may occur at the steel rim of the heavy vehicle in the range of $6.45 \cdot 10^5 - 8.75 \cdot 10^5$ cycles.

The mileage of the analyzed tipper truck was above 100 000 km. As the radius of the wheel was 0.5 m, the wheel rim analyzed withstood about $32 \cdot 10^6$ cycles and this means that the probability of reaching the fatigue limit in the rim material is very high.

The stresses in the rim are usually of a bending or complex nature [67]. Once the metallic material reaches its plastic *deformation limit, the discontinuity usually becomes a small* crack [67].

During the classical constant operation of vehicles, typical usage damages have resulted from material fatigue and can often appear in the characteristic locations of the so-called theoretical critical zones (TCZ). Unique situations are also possible, such as wheel collisions with an obstacle or a sudden puncture or tearing of the tire, causing permanent deformation of the wheel. During studies described in [76], such cases were omitted.

Based on the numerical analysis of stress in the model of the rim, three zones of increased concentration of stress were identified by Tarasiuk *et al*. [76] as being potential weak durability links, namely: the curving of the wheel rim, the boundary of weld cap and rim material and the area of the weld root joining the rim and disc.

To estimate the effect of material properties such as Yield Strength and Ultimate Strength and load on the achievement of fatigue strength in the rim material, a simplified Smith diagram was utilized [77–79].

The effect of the load was characterized by the values of von Mises stresses resulting from such a load in the rim material. The parameters for the mentioned diagram were estimated using equations given in [80–82].

The mean stress σ_m was defined by equation (6) [80]

$$\sigma_m = 0.5\,(\sigma_{\max} + \sigma_{\min})\,, \tag{6}$$

where: $\sigma_{\max}$ – maximum value of stress, $\sigma_{\min}$ – minimum value of stress.

The alternating stress also called the stress amplitude σ_a was defined by equation (7) [80]

$$\sigma_a = 0.5\,(\sigma_{\max} - \sigma_{\min})\,. \tag{7}$$

The stress ratio R was defined by equation (8) [81]

$$R = \sigma_{\max}/\sigma_{\min}\,. \tag{8}$$

The bending fatigue strength $S_{b,R=-1}$ for the stress ratio $R = -1 (\sigma_a = 0)$ was calculated from equation (9) [82]

$$S_{b,R=-1} = 0.47\,R_m\,. \tag{9}$$

As the Ultimate strength R_m of the analyzed steel was equal to 440 MPa, therefore the bending fatigue strength $S_{b,R=-1}$ was equal to 206.7 MPa

The bending fatigue strength $S_{b,R=0}$ for the stress ratio $R = 0$ ($\sigma_m = \sigma_a$) can be calculated from equation (10) [82]

$$S_{b,R=0} = 0.7\,R_m\,. \tag{10}$$

For the mentioned value of the ultimate strength R_m the bending fatigue strength $S_{b,R=0}$ was equal to 308 MPa.

As mentioned earlier, the Yield strength R_e for such steel reached a value of 300 MPa.

Therefore, the simplified Smith diagram for the analyzed steel was presented in Fig. 12. Three parameters: σ_{m1}, σ_{m2}, and σ_{m3} correspond to the values of the average von Mises stresses in the rim material selected in increasing order. The parameters σ_{a1}, σ_{a2}, and σ_{a3} corresponded to the stress amplitudes related to the mean stresses σ_{m1}, σ_{m2}, and σ_{m3}, respectively. The related bending fatigue strengths were marked as parameters S_{b1}, S_{b2}, and S_{b3}, respectively. The fatigue strength of the components/structural elements of the rim depends on various external and internal factors. Such factors were described in [83]. The external ones comprised shape and size, surface finish, and service conditions. The internal ones comprised compositions, microstructure, purity, and residual stresses. The internal factors can result from the heat-chemical treatment of the rim. To include the effect of such factors during the present analysis, it was assumed that their combined effect may be equivalent to the effect of doubling the value of the stress amplitude σ_a. It is visible that the fatigue strengths can reach values equal to, alternatively:

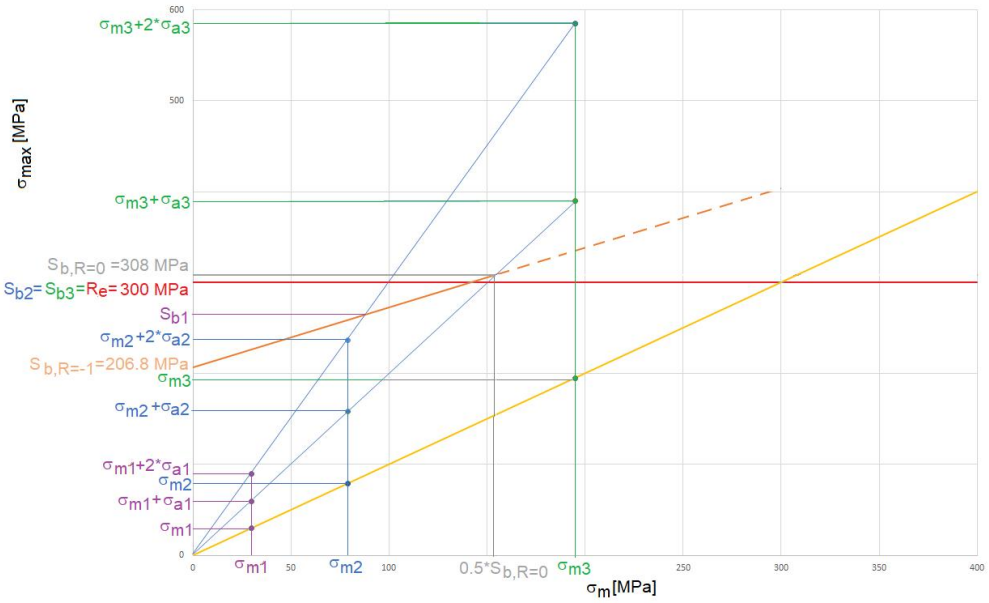

Fig. 12. The simplified Smith diagram for the steel analyzed

- The vertical coordinates of points lying on the limit line through the points $(0, S_{b,R=-1})$ and $(0.5 \cdot S_{b,R=0}, S_{b,R=0})$ on the simplified Smith diagram (Fig. 12)
- The Yield strength R_e if the latter is equal to or lower than values of such vertical coordinates.

4. RESULTS AND DISCUSSION

The obtained results were presented in three groups including the ones from:

- The observation of selected fragments of the damaged rim surface
- The measurement of the hardness and microscopic observations of the material structure
- The calculation of the torque loading the twin wheels of the tipper-truck rear axle
- The analysis of the stress distributions in the modelled rim

4.1. Observation results of selected fragments of the damaged rim surface

The obtained results from the observation of two selected fragments of the damaged rim surface were shown in Figs. 13 and 14. The first one comprised two zones (1 and 2) indicating the signs of fatigue wear. The second one comprised a zone indicating the presence of local overheating, as evidenced by bluish raids on the oxidized parts of the surface. It could be a result of the damaged rim fragment rubbing against each other or the twin wheel rim mounting bolts during the rolling of the wheel after bursting of its tire.

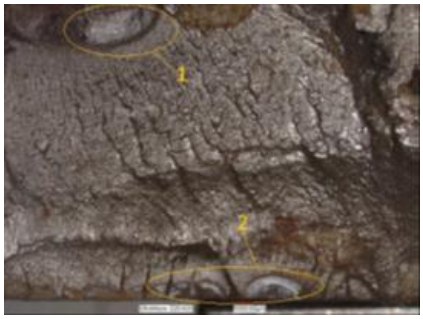

Fig. 13. View of the fracture surface of the damaged rim fragment with marked zones 1 and 2 indicating signs of fatigue wear

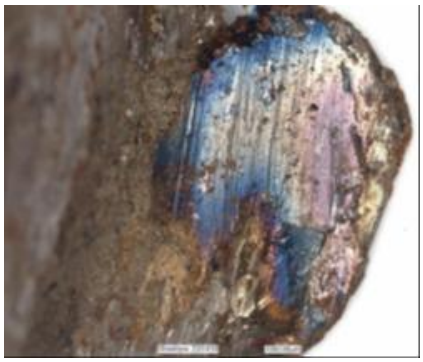

Fig. 14. View of the fracture surface of a fragment of the damaged rim with a zone indicating the presence of local overheating, as evidenced by bluish deposits on the oxidized parts of the surface

4.2. Results from the measurement of the hardness and microscopic observations of the material structure

Based on hardness measurements, it was found that the surface hardness of the rim is 152 HV10, while in the center of the rim cross-section, it is only 128 HV10. The calculated values of the fatigue strength σ_w for the measured values of hardness HV were presented in Table 1. The fatigue strength of the material near the surface zone was 1.14–1.26 higher than that of the core zone of the rim disc analyzed.

Table 1

The calculated values of the fatigue strength σ_w for the measured values of hardness HV

Hardness HV10	Fatigue strength σ_w [MPa]
152	243.2 ± 15.2
128	204.8 ± 12.8

Based on microscopic observations of the tested section of the rim material, the presence of a structure composed of ferrite and pearlite was found. While the structure is homogeneous in the areas just below the rim surface, in the middle of the cross-section there is a clear anisotropy in the distribution of ferrite and pearlite grains. In this case, the grains of both phases are arranged alternately, creating a characteristic stripe pattern. The obtained differences in the microstructure partially confirm that the rim disc was made of hot rolled steel. The comparison of microstructures from both analyzed areas is presented in Figs. 15 and 16.

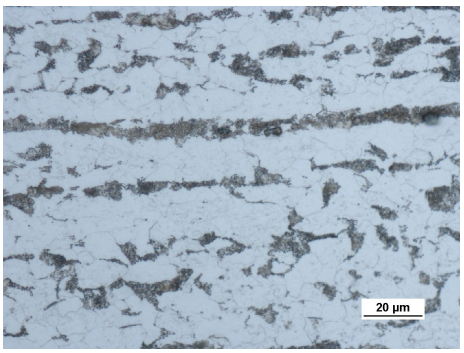

Fig. 15. The microstructure of the material sample in the measuring point 4 in Fig. 5

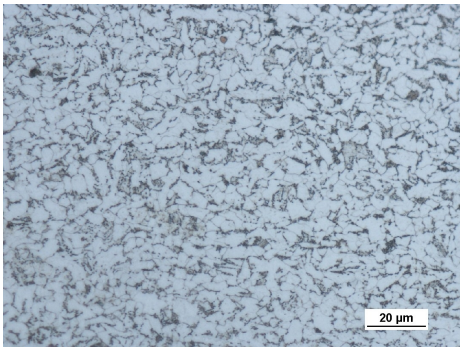

Fig. 16. The microstructure of the material sample in the measuring point 4 in Fig. 5

4.3. Calculated torque loading the twin wheels of the tipper-truck rear axle

The resulted values of the torque loading the twin wheels of the tipper-truck rear axle were presented in Table 2.

Table 2

The resulted values of the torque loading the twin wheels of the tipper-truck rear axle

Torque	Values [Nm]
$T_{\mathrm{ra-perm}}$	46240
$T_{\mathrm{ra}-M_{\max}}$	131256
$T_{\mathrm{ra}-P_{\max}}$	8640
$2 \cdot T_{\mathrm{ra-perm}}$	92480

During the transport of pallets with paving stones, the calculated values of maximal torque $T_{\mathrm{ra}-M_{\max}}$ exceeded these of the torque $2 \cdot T_{\mathrm{ra-perm}}$ transferrable by the twin wheel of the tipper-truck rear axle. This increases the risk of the occurrence of twin wheel slips relative to the road mated with it. Therefore, the torque $2 \cdot T_{\mathrm{ra-perm}}$ can be the maximal one transferable by this twin vehicle. Such a torque occurring during driving on the dirt road was 10.7-fold higher than the torque $2 \cdot T_{\mathrm{ra}-P_{\max}}$ occurring during driving on the asphalt road.

4.4. The stress distributions in the analyzed model of the rim

The effect of the average element size on the maximum value of von Mises stresses for different cases of loading of the twin wheel of the rear axle was shown in Table 3.

Table 3

The effect of the average element size on the maximum value of von Mises stresses for different cases of loading of the twin wheel of the rear axle. The maximum value of the von Mises stresses for the transport of pallets with paving stones during Case 1 – stop of the tipper-truck; Case 2 – driving on the asphalt road when both tires of each twin wheel of the rear axle were in contact with the road; Case 3 – driving on the dirt road when both tires of each twin wheel of the rear axle were in contact with the road; Case 4 – driving on the dirt road when case only one tire of the one twin wheel of the rear axle were in contact with the road

Average Element Size (as a fraction of bounding box length)	Case 1	Case 2	Case 3	Case 4
[%]	[MPa]			
10	30.44	31.08	72.79	183.7
5	35.97	42.37	112.7	279.2
3	51.34	57.06	121.9	298.9
2	55.34	60.19	158.8	389.6
1	56.52	61.17	161.12	415.2
0.5	57.06	61.94	163.04	431.5

It was assumed that the cases with Average Element Size as a 0.5% fraction of bounding box length were the optimal choices for the comparative analysis under the small costs of computation time and involvement of the computer RAM. It facilitated satisfying the important rule for grid generation that at least two finite elements per thickness, particularly that of the rims, should be applied to properly simulate the bending.

The obtained values of the von Mises stress distribution for the case of transport of pallets with paving stones during a stop of a tipper-truck were shown in Fig. 17. They hardly exceeded values of 57 MPa. In this case, both tires of each twin wheel of the rear axle were in contact with the road.

The obtained values of the von Mises stress distribution for the case of transport of pallets with paving stones during driving on the asphalt road were shown in Fig. 18. They did not exceed values of 61 MPa. In this case, both tires of each twin wheel of the rear axle were in contact with the road.

The obtained values of the von Mises stress distribution for the case of transport of pallets with paving stones during driving on the dirt road were shown in Fig. 19. They did not exceed values of 160 MPa. In this case, both tires of each twin wheel of the rear axle were in contact with the road as well.

The obtained values of the von Mises stress distribution for the case of transport of pallets with paving stones during driving on the dirt road were shown in Fig. 20. They did not exceed values of 400 MPa. In this case, only one tire of the one twin wheel of the rear axle was in contact with the road.

Although in most cases analyzed, the obtained values of the von Mises stresses did not exceed the value of the Yield Stress of assumed steel, in the last case they were higher than the Yield Stress by about 25%. Additionally, such stress values were 1.65-fold higher than the highest estimated value of the surface fatigue strength and the core fatigue strength presented in Table 1.

4.5. The fatigue in the analyzed model of the rim

For the values of von Mises stresses in the assembly of the modelled rims for the case of transport of pallets with paving stones during driving on the asphalt road when both tires of each twin wheel of the rear axle were in contact with the road the values of both mean stress σ_{m1} and stress amplitude σ_{a1} were equal to 30.1 MPa and the bending fracture strength S_{b1} from the simplified Smith diagram (Fig. 12) was equal to 272 MPa. This means that for the tipper-track operating under similar conditions the eventual fatigue failures can hardly be plastic.

For the values of von Mises stresses in the assembly of the modelled rims in the case of transport of pallets with paving stones while driving on a dirty road, when both tires of each twin wheel of the rear axle were in contact with the road the values of both mean stress σ_{m2} and stress amplitude σ_{a2} were equal to 79.4 MPa and the bending fracture strength S_{b2} from the simplified Smith diagram (Fig. 12) was equal to the Yield Strength R_e of 300 MPa. For the values of von Mises stresses in the assembly of the modelled rims in the case of transport of pallets with paving stones while driving on the dirt road when only one tire of one twin wheel of the rear axle was in contact with the road, the values of both mean stress σ_{m3} and stress amplitude σ_{a3} were equal to 195 MPa and the bending fracture strength S_{b3} from the simplified Smith diagram (Fig. 12) was equal to the Yield Strength R_e of 300 MPa.

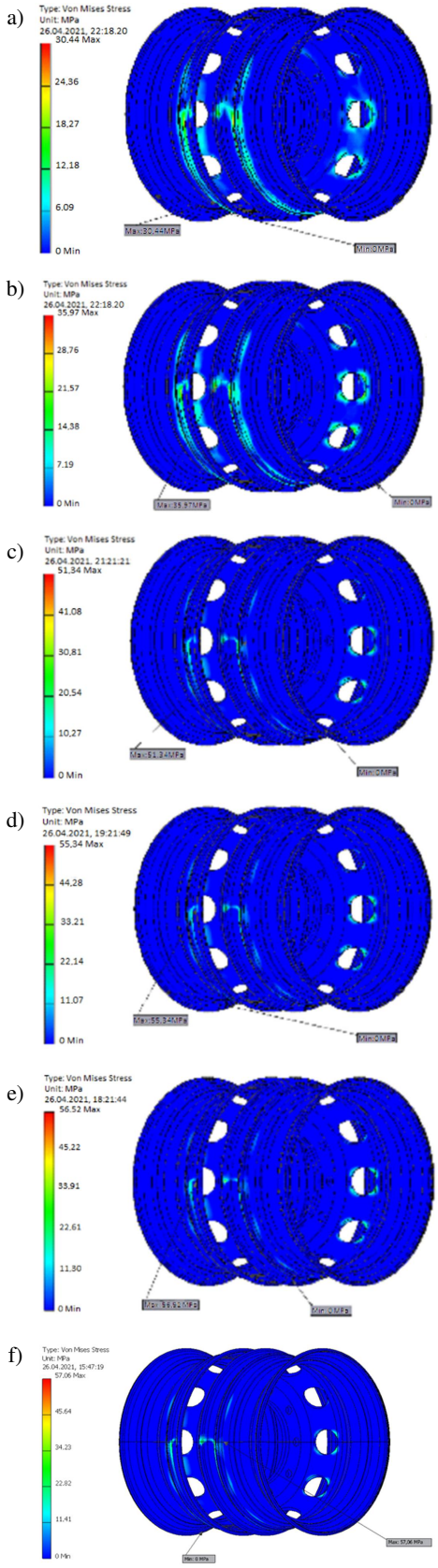

Fig. 17. The von Mises stress distribution in the assembly of the modelled rims for the case of transport of pallets with paving stones during stop of the tipper-truck. Average Element Size (as a fraction of bounding box length): a) 0.1; b) 0.05; c) 0.03; d) 0.02; e) 0.01; f) 0.005

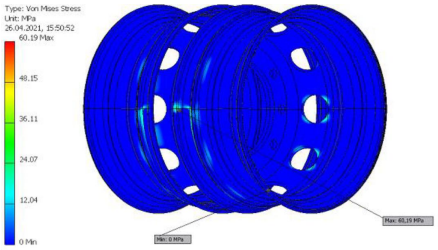

Fig. 18. The von Mises stress distribution in the assembly of the modelled rims for the case of transport of pallets with paving stones during driving on the asphalt road when both tires of each twin wheel of the rear axle were in contact with the road

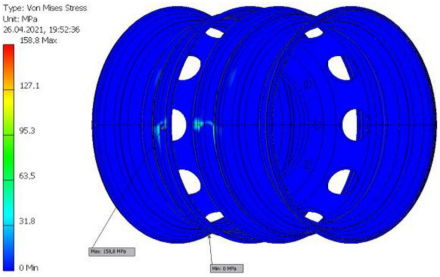

Fig. 19. The von Mises stress distribution in the assembly of the modelled rims for the case of transport of pallets with paving stones during driving on the dirt road when both tires of each twin wheel of the rear axle were in contact with the road

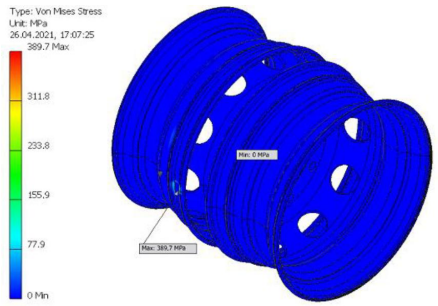

Fig. 20. The von Mises stress distribution in the assembly of the modelled rims for the case of transport of pallets with paving stones during driving on the dirt road when case only one tire of the one twin wheel of the rear axle were in contact with the road

The last two cases pointed out that for the tipper-track operating with a large share of similar conditions, eventual fatigue failures can be highly affected by the plastic strains.

5. CONCLUSIONS

Based on the results of the interview made with the participants of the road accident and the observation of the damaged rear twin wheel of the tipper-truck, the outer surfaces of the damaged rim fragments, the observation of the microstructures of the rim material sample, and the analysis of stresses in the models of the rim loaded according to the several analyzed scenarios, the following conclusions can be formulated:

- The rim disc material was made of hot-rolled weldable steel, as evidenced by the difference in microstructure in the rim material sample. The cut was made along the rim disc thickness at different depths from the surface.
- The damage to the rim was caused by the simultaneous influence of several factors, such as overloading the car, poor condition of the tires, loading the drive wheel by a part of the vehicle weight and the driving torque, as well driving over a pothole on a dirt road, causing a temporary relief of one of the tires in a twin wheel.
- Damage to the rim could have been caused due to the initiation and subsequent propagation of fatigue cracks, which could have been favored by:
  - the loosening of one of the bolts fixing the rims to the wheel hub,
  - the presence of material defects in the form of non-metallic inclusions or heterogeneous structure of the rolled steel of which the rim disc was made leading to the occurrence of local notches.
- Possible failure mechanism of the tire could relate to the damaged rim fragment rubbing against each other or against the twin wheel rim mounting bolts during the rolling of the wheel.
- Driving the highly loaded tipper-truck mainly on dirty roads strongly promotes the formation of fatigue failures in the wheel rims accompanied by plastic strains.
- Further studies should be directed to the effect of cornering and braking various tipper-truck configurations while driving on different roads and under different load conditions, also with its uneven distribution on the possible increase in load on individual tipper wheels.

REFERENCES

[1] "What Is Loose Cargo and Their Suitable Trailers?" [Online]. Available: https://www.haulio.io/blog/what-is-loose-cargo-and-suitable-trailers/ [Accessed: 15 March 2021].

[2] M. Rykala and L. Rykala, "Economic Analysis of a Transport Company in the Aspect of Car Vehicle Operation," *Sustainability*, vol. 13, no. 1, 427, 2021, doi: 10.3390/su13010427.

[3] H. Petroski, "To Engineer Is Human: The Role of Failure in Successful Design," St. Martin's Press, New York, N.Y., USA, 1985.

[4] H. Panjagala, M. Balakrishna, S. Kushnoore and E. Rohit, "Design & Weight Optimization of a Wheel Rim for Sport Utility Vehicle," in *MATEC Web Conf.*, vol. 172, 03006, 2018, doi: 10.1051/matecconf/201817203006.

[5] M. Carboni, S. Beretta, and A. Finzi, "Defects and in-service fatigue life of truck wheels," *Eng. Fail. Anal.*, vol. 10, pp. 45-57, 2003, doi: 10.1016/S1350-6307(02)00036-5.

[6] J.D. Varin, "Wheel Attachment Failures in Light-Duty Vehicles," *J Fail. Anal. Preven.*, vol. 17, pp. 660-671, 2017, doi: 10.1007/s11668-017-0297-0.

[7] J.C. Glennon, "Wheel and Hub Failures Analysis". [Online]. Available: http://www.crashforensics.com/wheelandhubfailures.cfm [Accessed on 22 April 2021].

[8] T.S. Prasad, T. Krishnaiah, J.M. Iliyas, and M.J. Reddy, "A Review on Modeling and Analysis of Car Wheel Rim using CATIA & ANSYS," *IJISME-India*, vol. 2, no. 6, pp. 1–5, 2014.

[9] L. Natrayan, P. Santhakumar, and R. Mohandass, "Design and Comparative Analysis of Old & New Model Car Wheel Rims with Various Materials," *IETE J. Res.*, vol. 2, no. 2, pp. 69–73, 2016.

[10] M. Sabri, M. Rezal, A. Mu'az, K. Shahril, and J. Ihsan, "Deformation Behaviour analysis of Car Wheel Rim under Different Loading Using Finite Element Method," *Int. J. Eng. Technol.*, vol. 5, no. 3, pp. 181–184, 2015.

[11] "Aluminum Automotive Manual 2015". [Online]. Available: https://www.european-aluminium.eu/resource-hub/aluminium-automotive-manual/ [Accessed: 17 March 2021].

[12] B. Zhang, S.L. Cockcroft, D.M. Maijer, J.D. Zhu, and A.B. Phillion, "Casting defects in low-pressure die-cast aluminum alloy wheels," *JOM*, vol. 57, pp. 36-43, 2005, doi: 10.1007/s11837-005-0025-1.

[13] M. Stańczyk and T. Figlus, "The Effect of Selected Parameters of Vibro-Abrasive Processing on the Surface Quality of Products Made of 6082 Aluminium Alloy," *Materials*, vol. 12, no. 24, 4117, 2019, doi: 10.3390/ma12244117.

[14] N. Satyanarayana and Ch. Sambaiah, "Fatigue Analysis of Aluminum Alloy Wheel Under Radial Load," *IJMIE-India*, vol. 2, no. 1, pp. 1–6, 2012.

[15] Das, Sourav. "Design and weight optimization of aluminum alloy wheel," *Int. J. Sci. Res.*, vol. 4, no. 6, pp. 1–12, 2014, doi: 10.29322/ijspr.

[16] S. Ganesh and P. Periyasamy, "Design and Analysis of Spiral Wheel Rim for Four Wheeler," *Int. J. Eng. Sci.*, vol. 3 no. 4, pp. 29–37, 2014.

[17] L. Wang, Y. Chen, C. Wang, and Q. Wang, "Fatigue Life Analysis of Aluminium Wheels by Simulation of Rotary Fatigue Test," *Strojniški vestnik–J. Mech. Eng.*, vol. 57, no. 1, pp. 31–39, 2011, doi: 10.5545/sv-jme.2009.046.

[18] A.I. Toulfatzis, M. Katsivarda, A. Rikos, A. Vazdirvanidis, and G. Pantazopoulos, "Failure and Fracture Analysis of Al-alloy Wheel Rim of a Vehicle," in *Proceedings of the 7th International Conference on Fracture Fatigue and Wear, July 2018*, Lecture Notes in Mechanical Engineering book series, 2018, doi: 10.1007/978-981-13-0411-8_3.

[19] Surasno and B. Tjahjohartoto, "Failure analysis of aluminum alloys casting in four-wheels vehicle rims," *IOP Conf. Ser.: Mater. Sci. Eng.,* vol. 980, 012004, 2020, doi: 10.1088/1757-899X/980/1/012004.

[20] S.-Y. Kwak, J. Cheng, and J-K. Choi, "Impact analysis of casting parts considering shrinkage cavity defect," *China Foundry*, vol. 8, no. 1, pp. 112–116, 2011.

[21] H. Liu, Y. Pan, H. Bian,, and C. Wang, "Optimize Design of Run-Flat Tires by Simulation and Experimental Research," *Materials*, vol. 14, no. 3, 474, 2021, doi: 10.3390/ma14030474.

[22] "The Pneumatic Tire. U.S". Department of Transportation, National Highway Traffic Safety Administration February 2006, DOT HS 810 561, 2006.

[23] I. Edunyah, "Causes of Tyre failure on Road Traffic Accident; A case study of Takoradi Township," *Int. J. Sci. Res. Publ.*, vol. 6, no. 2, pp. 30–35, 2016.

[24] M.J. Kalsher, M.S. Wogalter, K.R. Laughery, and R.W. Lim, "Consumer knowledge of tire maintenance and aging hazard," in *Proceedings of the Human Factors and Ergonomics Society Annual Meeting*, vol. 49, pp. 1757–1757, 2005, doi: 10.1177/154193120504901817.

[25] P. Baranowski and J. Malachowski, "Numerical study of selected military vehicle chassis subjected to blast loading in terms of tire strength improving," *Bull. Pol. Acad. Sci. Tech. Sci.*, vol. 63, no. 4, 867-pp. 878, 2015, doi: 10.1515/bpasts-2015-0099.

[26] Z. Zhenglong, S. Bin, L. Jiangang, D. Zhiuguang, and H. Zhongbo, "Research on ride comfort performance of a metal tire," *Bull. Pol. Acad. Sci. Tech. Sci.*, vol. 68, no. 3, pp. 491–502, 2020, doi: 10.24425/bpasts.2020.133384.

[27] A. Weyssenhoff, M. Opala, S. Koziak, and R. Melnik, "Characteristics and investigation of selected manufacturing defects of passenger car tires," *Transp. Res. Proc.*, vol. 40, pp. 119–126, 2019, doi: 10.1016/j.trpro.2019.07.020.

[28] T.D. Gillesipie, "Relationship of Truck Tire/Wheel Nonuniformities to Cyclic Force Generation," Final report UMTRI-84-18, April 1984.

[29] J. Suffeleers, "Tyre non-uniformities and their effect on chassis vibrations," Master's thesis, Technische Universiteit Eindhoven, 2010.

[30] H.R. Dorfi, "Tire Non-Uniformities and Steering Wheel Vibrations," *Tire Sci Technol.*, vol. 33, no. 2, pp. 64–102, 2005, doi: 10.2346/1.2186787.

[31] R. Sivinski, "Evaluation of the effectiveness of tpms in proper tire pressure maintenance," Technical report, NHTSA 2012.

[32] E. Euchler, O. Kratina, R. Stoček, and M. Gehde, "A Study of Correlation between Crack Initiation during Dynamic Wear Process and Fatigue Crack Growth of Reinforced Rubber Materials," in *European Symposium on Friction, Wear, and Wear Protection*, 2015, 525274, doi: 10.1155/2015/525274.

[33] S.Z. Zhang, Y.H. Wu, and J. Chang, "Design of Tire Damage Image Recognition System Based on Deep Learning," *J. Phys.: Conf. Ser.*, vol. 1631, 012015, 2020, doi: 10.1088/1742-6596/1631/1/012015.

[34] J. Siegel, Y. Sun, and S. Sarma, "Automotive Diagnostics as a Service: An Artificially Intelligent Mobile Application for Tire Condition Assessment," in *International Conference on AI and Mobile Services*, Seattle, USA, June 2018.

[35] K.R.S. Wright and P.S. Els, "The Effects of Age on the Stiffness Properties of a SUV Tyre," in *19th International & 14th European-African Regional Conference of the ISTVS*, Budapest, September 25–27, 2017, doi: 10.5281/zenodo.1059043.

[36] "FTire – Flexible Structure Tire Model. Modelization and Parameter Specification," Cosin Scientific Software AG, Muenchen, Germany. [Online]. Available: https://www.cosin.eu/wp-content/uploads/ftire_model.pdf [Accessed: 22 April 2021].

[37] "Tires: Your safety and your life are riding on them," Safety 1(3) June 2013. [Online]. Available: https://one.nhtsa.gov/nhtsa/safety1nnum3ers/june2013/9719_images/9719_S1N_Tires_Nwsltr_June13_062713_v4_tag.pdf [Accessed: 22 April 2021].

[38] P. Balderstone, A. Livadeas, and A. Wilson-Law, "Tyre Ageing: its effect on material properties and structural integrity," Published Project Report PPR904, Department for Transport (DfT) contract ref P4102035, 9th May 2019.

[39] J.P. Pauwelussen, W. Dalhuijsen, and M. Merts, "Tyre dynamics, tyre as a vehicle component Part 1.: Tyre handling performance," *VERT*, FI-04-B-F-PP-160531, HAN University, 2007.

[40] R. Rajamani, N. Piyabongkarn, J. Lew, and K. Yi, "Phanomchoeng, G. Tire-Road Friction-Coefficient Estimation," *IEEE Contr. Syst. Mag.*, vol. 30, no. 4, pp. 54–69, 2010, doi: 10.1109/MCS.2010.937006.

[41] R. Ghandour, A. Victorino, M. Doumiati, and A. Charara, "Tire/road friction coefficient estimation applied to road safety," in 18th *Mediterrian Conf. Control Automation, MED'10*, Marrakech, Morocco, 2010, pp. 1485–1490.

[42] D. Fodor, K. Enisz, R. Doman, and P. Toth, "Tire Road friction coefficient estimation methods comparison based on different vehicle dynamics models," in *2011 IEEE Vehicle Power and Propulsion Conference, 2011*, USA, 2011, pp. 1–4, doi: 10.1109/VPPC.2011.6043067.

[43] Y. Chen and J. Wang, "Vehicle-longitudinal-motion-independent real-time tire-road friction coefficient estimation," in *Proc. 49th IEEE Conference on Decision and Control (CDC)*, USA, 2010, pp. 2910–2915, doi: 10.1109/CDC.2010.5717437.

[44] Y. Chen and J. Wang, "Adaptive Vehicle Speed Control with Input Injections for Longitudinal Motion Independent Road Frictional Condition Estimation," *IEEE Trans. Veh. Technol.*, vol. 60, no. 3, pp. 839–848, 2011, doi: 10.1109/TVT.2011.2106811.

[45] C. Ahn, H. Peng, and H.E. Tseng, "Robust estimation of road friction coefficient," in *Proc. 2011 American Control Conference*, USA, 2011, pp. 3948–3953, doi: 10.1109/TCST.2011. 2170838.

[46] R. Rajamani, G. Phanomchoeng, D. Piyabongkarn, and J.Y. Lew, "Algorithms for Real-Time Estimation of Individual Wheel Tire-Road Friction Coefficients," *IEEE ASME Trans. Mechatron.*, vol. 17, no. 6, pp. 1183–1195, 2012, doi: 10.1109/TMECH.2011.2159240.

[47] Q. Cheng, A. Correa-Victorino, and A.A. Charara, "A new nonlinear observer using unscented Kalman filter to estimate sideslip angle, lateral tire road forces and tire road friction coefficient," in *2011 IEEE Intelligent Vehicles Symposium (IV)*, Germany, 2011, pp. 709–714.

[48] R. de Castro, R.E. Araujo, J.S. Cardoso, and D.A. Freitas, "A new linear parametrization for peak friction coefficient estimation in real time," in *2010 IEEE Vehicle Power and Propulsion Conference*, France, 2010, pp. 1–6, doi: 10.1109/VPPC.2010.5729138.

[49] C.-S. Liu, "Adhesion coefficient of automobile tire and road surface," *J. Cent. South Univ. Technol.*, vol. 15, no. s1, pp. 210–214, 2008, doi: 10.1007/s11771-008-0348-5.

[50] J.Y., Wong, *Theory of ground vehicles*. 2nd ed., John Wiley & Sons, 1993.

[51] H. Bauer, Arne Cypra, Anton Beer, and Robert Bosch GmbH, *Automotive Handbook*. 4th ed., Stuttgart: Robert Bosch, Warrendale, PA, USA, 1996.

[52] J. Cabrera, J. Castillo, J. Fernández, J.M. Velasco García, A. Guerra, and P. Hernández, "A Procedure for Determining Tire-Road Friction Characteristics Using a Modification of the Magic Formula Based on Experimental Results," *Sensors*, vol. 18, no. 3, 896, 2018, doi: 10.3390/s18030896.

[53] M. Acosta, S. Kanarachos, and M. Blundell, "Road Friction Virtual Sensing: A Review of Estimation Techniques with Emphasis on Low Excitation Approaches," *Appl. Sci.*, vol. 7, 1230, 2017, doi: 10.3390/app7121230.

[54] Y. Lian, Y. Tian, L. Hu, and C. Yin, "Development of identification of tire-road friction conditions," in *12-th ICARCV*, China, 2012, pp. 1812–1817, doi: 10.1109/ICARCV.2012.6485425.

[55] G. Erdogan, L. Alexander, and R. Rajamani, "Estimation of Tire-Road Friction Coefficient Using a Novel Wireless Piezoelectric Tire Sensor," *IEEE Sens. J.*, vol. 11, no. 2, pp. 267–279, 2011, doi: 10.1109/JSEN.2010.2053198.

[56] G. Erdogan, L. Alexander, and R. Rajamani, "Adaptive Vibration Cancellation for Tire-Road Friction Coefficient Estimation on Winter Maintenance Vehicles," *IEEE Trans. Control Syst. Technol.*, vol. 18, no. 5, pp. 1023–1032, 2010, doi: 10.1109/TCST.2009.2031326.

[57] K.B. Singh and S. Taheri, "Estimation of tire–road friction coefficient and its application in chassis control systems," *Syst. Sci. Control Eng.*, vol. 3, no. 1, pp. 39–61, 2015, doi: 10.1080/21642583.2014.985804.

[58] C. Lex, "Estimation of the Maximum Coefficient of Friction between Tire and Road Based on Vehicle State Measurements," Doctoral Thesis. Graz University of Technology, Faculty of Mechanical Engineering and Economic Sciences, 2015.

[59] J.C. Pang, S.X. Li, Z.G. Wang, and Z.F. Zhang, "Relations between fatigue strength and other mechanical properties of metallic materials," *Fatigue Fract. Eng. Mater. Struct.*, vol. 37, pp. 958–976, 2014, doi: 10.1111/ffe.12158.

[60] "Mercedes Actros 4143 K 8X4 Tipper Truck. Bas Trucks." [Online]. Available: https://www.bastrucks.com/vehicles/used/truck-tipper-mercedes-actros-4143-k-2002-8x4-94145 [Accessed: 17 March 2021].

[61] "Mercedes-Benz Powertrain. Truck Classic Engines." [Online]. Available: https://www.mercedes-benz.com/en/vehicles/aggregates/powertrain-truck-classic-engines/ [Accessed: 17 March 2021].

[62] "Mercedes-Benz Actros Specification." [Online]. Available: http://www.zimoco.co.zw/wp-content/uploads/2016/10/MBSA ActrosSpecificationFA1.pdf [Accessed: 17 March 2021].

[63] "14.00R20 Michelin XZL Complete on Wheel 164/160G TL." [Online]. Available: https://www.heuver.com/product/B014000 20MIGXZL54/14-00r20-michelin-xzl-complete-on-wheel-164-160g-tl [Accessed: 17 March 2021].

[64] "EMBAR®steel AS/NZS 3679.1-300 – BlueScope Steel, Uncoated Steel Data Sheet, February 2018. EmbarDatasheet.pdf." [Online]. Available: http://steel.com.au/products/uncoated-steel/embar-steel [Accessed: 17 March 2021].

[65] J. Shinde, S. Kadam, and S. Pandit, "Review Paper on Design and Analysis of Automotive Wheel Rim Using Finite Element Analysis," *Int. Res. J. Eng. Technol.*, vol. 4, no.7, pp. 2723–2725, 2017.

[66] A.S. Karthik, S. Praveen Ullagaddi, P. Sangangouda, J. Chandankumar, and H. Dayanand, "Static Analysis of Alloy Wheel using FEA," *Int. J. Innov. Res. Sci. Technol.*, vol. 2, no. 12, pp. 397–401, 2016.

[67] X. Jiang, R. Lyu, Y. Fukushima, M. Otake, and D.Y. Ju, "Lightweight design and analysis of automobile wheel based on bending and radial loads," *IOP Conf. Ser.: Mater. Sci. Eng.*, vol. 372, 012048, 2018, doi: 10.1088/1757-899X/372/1/012048.

[68] Rim B. Venkat Vinay Kumar, and K. Devaki Devi, "Design Analysis and Optimization of a Wheel," *Int. J. Anal. Exp. Modal Anal.*, vol. 11, no. 9, pp. 1879–1886, 2019.

[69] Kalpesh R. Salunkhe, and Shailesh S. Pimpale, "Design, FEM Analysis and of Alloy Wheel Rim of a Four Wheeler," *Int. Adv. Res. J. Sci. Eng. Technol.*, vol. 4, no. 9, 229–235, 2017. doi: 10.17148/IARJSET.2017.4931.

[70] Priyanka Mhaske, P.N. Narwade, and M.P. Nagarkar, "Analysis of Vertical Stiffness of Passenger Car Tire at Different Pressure using FE Model," *IJIERT, ICITDCEME'15 Conf. Proc.*, 2015, pp. 1–6.

[71] R. Hidayat, S.E. Pranoto, M. Tauviqirrahman, and A.P. Bayuseno, "Stress investigation on the rolling tires across the speed bump using finite element method," *AIP Conf. Proc.*, vol. 1725, 020028, 2016, doi: 10.1063/1.4945482.

[72] J. Stearns, T.S. Srivatsan, X. Gao, and P.C. Lam, "Understanding the Influence of Pressure and Radial Loads on Stress and Displacement Response of a Rotating Body: The Automobile Wheel," *Int. J. Rotating Mach.*, vol. 2006, 60193, pp. 1–8, 2006, doi: 10.1155/IJRM/2006/60193.

[73] V. Kazymyrovych, "Very high cycle fatigue of engineering materials. A literature review," Research Report, Karlstad University Studies, 22, 2009.

[74] S.M. Sachin, L.K. Sayed, and L.B. Sayyad, "Static and Fatigue Analysis of Automotive Wheel Rim," *IRJET*, vol. 2, no. 5, pp. 753–758, 2015.

[75] M.M. Topaç, S. Ercan, and N.S. Kuralay, "Fatigue life prediction of a heavy vehicle steel wheel under radial loads by using finite element analysis," *Eng. Fail. Anal.*, vol. 20, pp. 67–79, 2012, doi: 10.1016/j.engfailanal.2011.10.007.

[76] W.D. Callister Jr. and D.G. Rethwisch, "Materials Science and Engineering," 9th ed., John Wiley & Sons, 2014.

[77] P. Tarasiuk, K.L. Molski, and A. Szymaniuk, "Fatigue designing of welded agricultural wheels," *Eksploat. Niezawodn.*, vol. 15, no. 2, pp. 123–128, 2013.

[78] J. Kunz, "Festigkeitsbedingung bei schwingender Belastung mit Kerbwirkung / Strength Conditions at Oscillating Load with Notch Effect, Konstruktion," *Konstruktion (Berlin) [DE-600]*, vol. 7/8, pp. 74–82, 2015.

[79] D.T. Jelaska, "Fatigue assessment for combined HCF/LCF loading," *Proc. ASME 2002 International Mechanical Engineering Congress and Exposition. Recent Advances in Solids and Structures.*, 2002, pp. 135–139, doi: 10.1115/IMECE2002-32304.

[80] D. Jelaska, S. Glodež, and S. Podrug, "Closed form expression for fatigue life prediction at combined HCF/LCF loading," *Facta Univ. Mech. Autom. Control Robot.*, vol. 3, no. 13, pp. 635–646, 2003.

[81] M. Gedeon, "Mean Stress and Alternating Stress," *Materion Brush Performance Alloys. Technical Tidbits*, vol 3, no. 63, 2014. [Online]. Available: https://materion.com/-/media/files/alloy/newsletters/technical-tidbits/issue-no-63—mean-stress-and-alternating-stress.pdf [Accessed: 22 April 2021].

[82] A. Wan *et al.*, "High-cycle fatigue behavior of Co-based superalloy 9CrCo at elevated temperatures," *Chin. J. Aeronaut.*, vol. 29, no. 5, pp. 1405–1413, 2016, doi: 10.1016/j.cja.2016.01.009.

[83] I. Tylek and K. Kuchta, "Mechanical Properties of Structural Stainless Steels," *Tech. Trans. Civ. Eng. – Krakow*, vol. 4–B, pp. 59–80, 2014.

[84] A. James, "Eight factors affecting the fatigue strength of metal materials," 2021. [Online]. Available: https://www.linkedin.com/pulse/eight-factors-affecting-fatigue-strength-metal-materials-marco-xiong/ [Accessed: 22 April 2021].